Science and Technology for Energy Transition 80, 10 (2025)

https://doi.org/10.2516/stet/2024108

Available online at:
stet-review.org

Research Article — Open Access

Distributed robust Volt-VAr control strategy for accurate reactive power sharing in islanded microgrid

Pradeep Kumar Singh and Dharmendra Kumar Dheer*

Department of Electrical Engineering, National Institute of Technology Patna, 800005 Bihar, India

Received: 23 August 2024 / Accepted: 28 November 2024

Abstract. This paper introduces a novel Distributed Robust Volt-VAr Control Strategy (DRVVCS) aimed at achieving accurate proportional reactive power sharing in islanded microgrids, emphasizing adaptability, simplicity, and reduced reliance on communication. This scheme also enhances the flexibility and scalability of the system, which are generally challenging in distributed control schemes. The system's seamless transition between different network topologies and accurate reactive power sharing under varying loads with suggested DRVVCS are evaluated through comprehensive simulations. The proposed scheme is also tested on a standard IEEE 33-bus system with three sources and a standard IEEE 69-bus system with three and five sources to observe its effectiveness in different operating scenarios. The proposed DRVVCS is compared with conventional droop control and other existing methods to showcase its effectiveness and versatility.

Keywords: Islanded microgrid, Distributed Robust Volt – VAr control strategy, Droop control, Reactive power sharing, Reactive power error.

1 Introduction

Islanded microgrids have garnered substantial attention in recent years for their remarkable ability to provide reliable and resilient power supply, particularly in isolated areas or during grid outages. Effective scheduling of distributed energy resources plays a crucial role in improving the economic and environmental sustainability [1]. The Reactive power management is necessary for maintaining voltage stability and ensuring efficient operation of islanded microgrids. The effective sharing of power among Distributed Energy Resources (DERs) within the microgrid for different loading conditions such highly reactive load or evolving load like electric vehicle [2] is essential for maintaining stability, minimizing power losses, avoiding the overloading of smaller sources and helps in minimizing the circulating currents.

Various control techniques have been proposed in the literature to achieve proportional power sharing among the Distributed Generators (DGs) in islanded microgrids. These techniques include conventional droop control, modified droop control, virtual impedance control, centralized control, and distributed control, among others [3–6]. The conventional droop control methods have been widely explored by researchers [7, 8], to achieve proportional power sharing in islanded microgrids. These methods shares proportional active power accurately but often fall short when it comes to sharing reactive power proportionally. In order to address this limitation, adaptive droop coefficient-based methods have been presented in [9–14], aiming to improve reactive power sharing in islanded microgrids.

A self-adjusting droop control strategy is proposed in [9] and further modified in [10] and [11] to reduce error in reactive power sharing in islanded microgrids. Despite significant improvements, achieving accurate proportional reactive power sharing remains a challenge. In [12] the authors proposed a dispatchable droop control method that improves reactive power sharing among Distributed Generators (DGs), but it introduces additional complexity by incorporating a Proportional-Integral (PI) controller. In contrast, a simplified control scheme is suggested in [13] however, it fails to detect load changes below a certain threshold employed in the research. Although adaptive droop coefficient-based methods have shown significant improvements in reactive power sharing, they still fall short of meeting the permissible limits, leaving room for further enhancement. In [15], a small signal injection-based technique with virtual impedance adjustment is used to enhance performance, while authors in [16] introduces an advanced droop control strategy that requires measurements of Point of Common Coupling (PCC) voltage but lacks accuracy. Authors in [17] proposed Energy Management System

* Corresponding author: dkdheer@nitp.ac.in

(EMS) and a Sliding Mode Control (SMC) to improve accuracy in power sharing and improve the quality of the voltage, but high frequency oscillations that occurs around the sliding surface can lead to excessive switching of power electronics devices causing increased wear and tear. Authors in [18] proposed artificial gorilla troops algorithm for enhancing decentralized frequency regulation approach in mixed source of generation diversified with wind and PV integration while authors in [19] presented various frequency stability control strategies for microgrid based on hybrid renewable energy. Authors in [20] suggested the use of both voltage and current control modes of inverters simultaneously which is relatively complicated and potentially incurring a heavy computational burden for the controller.

Virtual impedance (Z_v) based method presented in [21, 22] addresses mismatch in feeder impedances by incorporating a sufficiently high fixed virtual impedance in the outer voltage control loop, considering stability, transient response, and power flow constraints. However, changes in network topology, such as DER additions or removals, can significantly impact the effectiveness, requiring continuous adjustment and reconfiguration, leading to complexity and time-consumption. To tackle the limitations associated with the fixed (Z_v) authors in [23–30] proposed adaptive (Z_v) methods to improve the reactive power sharing among the DGs. A Disturbance Observer (DOB) based novel power sharing scheme is proposed by the authors in [23] for reactive power sharing but the proposed scheme is applicable to small-scale microgrids only. Authors in [24] presented an adaptive decentralized technique for adjusting the virtual impedance. Virtual impedance is adjusted based on its output current in this case, without the need of communication, extra sensors or network parameter/load estimations but proportional reactive power sharing is not achieved accurately. Authors in [25] suggested an iterative virtual impedance regulation (IVIR) strategy in which fixed virtual impedance and adaptive virtual impedance regulation are combined, but the proposed method is complex and has large settling time. Authors in [26] examines the power sharing performance among droop controlled inverters and virtual synchronous generators in a system with mixed tie-line configurations. Virtual impedance optimization technique is used in [27], while authors in [28, 29] used online estimation technique to find out the value of virtual inductance and authors in [30] proposed a control scheme which uses three nested loops. All these techniques require extensive computation and complex to implement.

While the adaptive virtual impedance method offers the potential for improved reactive power sharing in islanded microgrids, it faces the challenges such as complexity, computational burden, stability issues and limited effectiveness under dynamic and transient conditions. Microgrid Central Controller (MGCC) based control schemes are presented by the authors in [31–33] to improve reactive power sharing among the sources. Although MGCC based control schemes significantly improves the reactive power sharing among the DGs, it has to deal with challenges such as communication dependency, scalability, complexity and computational burden. To reduce the dependency on the communication authors in [34–47] proposed distributed control strategies based on consensus and secondary control for accurate reactive power sharing in islanded microgrid. The consensus-based control scheme was proposed by the authors in [34, 35] but the former is applicable for radial network only. The control scheme proposed by the authors in [36] is complex and applicable to balanced microgrid only, while the control method proposed by the authors in [37] do not consider meshed network configurations, affecting their plug-and-play capability. Control method proposed by the authors in [38] rely on strong communication, which can pose challenges in practical microgrid implementations. Distributed event-triggered control scheme is proposed by the authors in [39] which shares almost accurate reactive power and reduces the communication burden but it requires addition PI controller. A consensus-based Multiagent System (MAS) is suggested by the authors in [40] to restore voltage/frequency deviations and enable true power sharing. The proposed method uses PI and ANN in secondary control along with PR controller in primary control making it complex and computationally extensive. Authors in [41] proposed containment and consensus-based method while authors in [42] adaptively regulate the virtual impedance using a first-order consensus algorithm to achieve bounded voltage and precise reactive power sharing in islanded ac microgrids. Strategy suggested by [43] uses three control layer making it complex and increases dependency on communication. A distributed virtual negative sequence impedance control based on consensus is proposed in [44], while authors in [45] proposed two layer control scheme for proportional reactive power sharing among the sources. The control scheme proposed by the authors in [46] uses secondary control along with online optimization to reduce computational burden. Distributed Self-triggered control method is proposed by the authors in [47] to further reduce the communication bandwidth and computational burden associated with distributed control schemes.

Based on the literature it was observed that decentralized control schemes, while appealing due to their simplicity and practical implementation, fall short when it comes to accurately sharing proportional reactive power. On the other hand, centralized control methods exhibit the desired accuracy in reactive power sharing, but their heavy reliance on robust communication poses significant challenges in practical implementation. Bridging this gap, researchers have proposed distributed control schemes, aimed at reducing communication dependency while maintaining effective reactive power sharing. However, these approaches face challenges related to communication and synchronization, requirement of secondary control, scalability and complexity, sensitivity to network conditions, and lack of adaptability. In order to ensure the seamless and efficient operation of an islanded microgrid, the control scheme should adhere to the following imperative conditions:

- Accurate proportional real and reactive power sharing.
- The control scheme should be simple and easy to implement practically.
- It should work effectively under all loading condition including light and heavy load cases.
- Minimal dependency on communication.

- Independent to network information such as feeder impedance, location of load and size of DGs to allow plug and play.
- Fast response and ability to detect small and continuous load changes.
- It should be least dependent on optimization and approximation so that computational burden can be reduced.
- Independent to network configuration including radial network, reconfigured network and meshed network *etc.*

Despite extensive research on reactive power sharing, it is evident that existing control schemes do not fully meet all the aforementioned requirements. Therefore, there is a need for improved control strategy to effectively address these issues. This paper introduces a controller that fine-tunes the nominal voltage to achieve precise proportional reactive power sharing, all while keeping the output voltage within desired limits. The proposed method is simple to implement and work effectively irrespective to the load type, load location and network configuration. The proposed method uses low bandwidth, one way communication, hence communication dependency is minimal.

The rest of the paper is organised as follows: The proposed DRVVC and system used in this study is presented in Section 2. Section 3 contains MATLAB simulink study to validate the claims of the proposed control scheme. Generation of multiplication factor M_{fc} and tuning of control parameter β is discussed in Section 4 and overall conclusion of this study is presented in Section 5.

2 Proposed control scheme and system under study

The Conventional Droop Control Strategy (CDCS) for proportional real and reactive power sharing among the DGs is as follows [7]:

$$\omega^* = \omega_n - m_p P_c, \tag{1}$$

$$\begin{array}{c} V^*_{\rm odr} = V_n - n_q Q_c \\ V^*_{\rm oqr} = 0 \end{array}, \tag{2}$$

where, ω^* is the reference frequency in rad/s, ω_n is the nominal frequency in rad/s, m_p is real power droop coefficient in rad/W-s and P_c is instantaneous filtered active power. $V^*_{\rm odr}$ is d-axis reference voltage, $V^*_{\rm oqr}$ is q-axis reference voltage, V_n is the nominal voltage, n_q is the reactive power droop coefficient in V/VAr and Q_c is instantaneous filtered reactive power.

P_c and Q_c is clean power obtained by passing the instantaneous active power (p) and instantaneous reactive power (q) through a low pass filter given as:

$$P_c = \frac{\omega_c}{s+\omega_c} p, \tag{3}$$

$$Q_c = \frac{\omega_c}{s+\omega_c} q, \tag{4}$$

where, ω_c is cut of frequency of low pass filter in rad/s. With the help of locally measured $v_{\rm odq}$ and $i_{\rm odq}$, p and q can be calculated as:

$$p = 1.5(v_{\rm od} i_{\rm od} + v_{\rm oq} i_{\rm oq}), \tag{5}$$

$$q = 1.5(v_{\rm oq} i_{\rm od} - v_{\rm od} i_{\rm oq}). \tag{6}$$

It is well known that the conventional droop control is able to share active power proportionally but it fails to share the proportional reactive power among the DGs because of its association with difference in feeder impedance, asymmetry in load magnitude, and load location.

To overcome the limitations of conventional droop control an adaptive nominal voltage based control scheme is proposed in this work, which is given as:

$$V^*_{\rm odr} = \gamma {\rm M_{fc}} V_n - n_q Q, \tag{7}$$

where, γ is an unit-less factor which is defined as follows:

$$\gamma = \frac{\beta + V_{\rm odr-pu}}{1 + \beta I_{\rm odr-pu}}. \tag{8}$$

Here, β is tuning parameter, $V_{\rm odr-pu}$ is d-axis component of reference voltage in pu, $I_{\rm odr-pu}$ is d-axis component of reference current in pu, and $M_{\rm fc}$ is common multiplying factor through a very low bandwidth, one way communication channel. The $V_{\rm odr\text{-}pu}$ and $I_{\rm odr\text{-}pu}$ can be calculated as follows:

$$V_{\rm odr-pu} = \frac{V^*_{\rm odr}}{V_n}, \tag{9}$$

$$I_{\rm odr-pu} = \frac{I^*_{\rm odr}}{I_o}. \tag{10}$$

It is to be noted that $V^*_{\rm odr}$ and $I^*_{\rm odr}$ used in equations (9) and (10) are the values from previous sampling cycle and $I_{\rm o}$ is output current.

2.1 System under study: (Low voltage microgrid)

To study the performance of the proposed control method, it is tested on three equally rated DGs with two types of test systems named as Test configuration-1 (Fig. 1), containing common load and local load and Test configuration-2 (Fig. 2), comprising loads of different magnitudes at different locations along with switches that allow it to work in various network configurations, including radial network, reconfigured network, and mesh network. The line and load data corresponding to the test systems are given in Tables 1 and 2, along with switch positions for various network configurations as shown in Table 3.

2.2 System under study: (Practical system)

The proposed method's performance was rigorously evaluated on IEEE standard test systems, demonstrating its effectiveness and robustness.

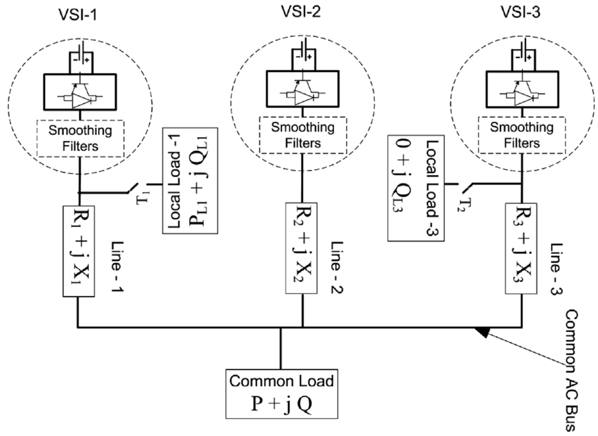

Figure 1. Low voltage microgrid: Test Configuration-1.

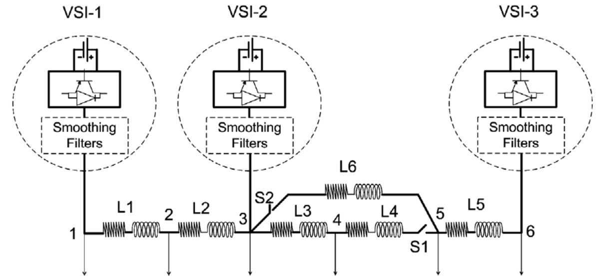

Figure 2. Low voltage microgrid: Test Configuration-2.

Table 1. Line and load data of test configuration-1.

Line no.	Impedance (Ω)	R/X ratio	Connected load (kVA)
Line-1	0.20 + j 0.06	3.33	Common load = 10 + j 5.0
Line-2	0.30 + j 0.09	3.33	Local load-1 = 2.0 + j 1.0
Line-3	0.40 + j 0.12	3.33	Local load-2 = 0.0 + j 5.0

Table 2. Line and load data of test configuration-2.

Line no.	Impedance (Ω)	R/X ratio	Node no.	Connected load (kVA)
L1	0.10 + j 0.08	1.25	1	3.0 + j 1.0
L2	0.20 + j 0.35	0.57	2	1.0 + j 0.3
L3	0.15 + j 0.19	0.79	3	5.0 + j 4.0
L4	0.20 + j 0.10	2.00	4	1.0 + j 2.0
L5	0.18 + j 0.25	0.72	5	1.0 + j 0.1
L6	0.15 + j 0.16	0.94	6	3.0 + j 2.0

2.2.1 IEEE 33 bus system

An islanded IEEE 33 bus system is shown in Figure 3 and its load and line data is taken from [48]. In Figure 3, bus numbers are marked to the left side and line numbers are marked to the right side. There are total five tie lines (shown by dotted lines) are present in the system and three DGs *i.e.* DG-1, DG-2 and DG-3 are connected at bus 6, 30 and 14 respectively.

2.2.2 IEEE 69 bus system

The line and load data of the IEEE 69 bus system shown in Figure 4 is adopted from [49]. The node numbers are marked below the nodes and line numbers are marked above lines in Figure 4. Dotted lines indicate the tie lines, and DG-4 and DG-5 are linked to switches S-1 and S-2. DG-1 is connected to bus 61, DG-2 to bus 17, and DG-3 to bus 11. When operating with all five DGs, closing switches S-1 and S-2 will connect DG-4 to bus 45 and DG-5 to bus 49.

Table 3. Switch positions among various network configurations for test configuration-2.

Topology	Switch position
Radial network	S1: Close, S2: Open
Reconfigured network	S1: Open, S2: Close
Meshed network	S1: Close, S2: Close

3 Simulation studies

To validate the effectiveness and achieved accuracy in Q_{sh} among the DGs, real time simulation is performed using MATLAB/Simulink. To gain deeper insights into the efficacy of DRVVCS, it undergoes a comprehensive comparison with the conventional droop control strategy [7] across both test configurations illustrated in Figures 1 and 2. In the context of a microgrid with p-equally rated sources, one can derive the anticipated reactive power

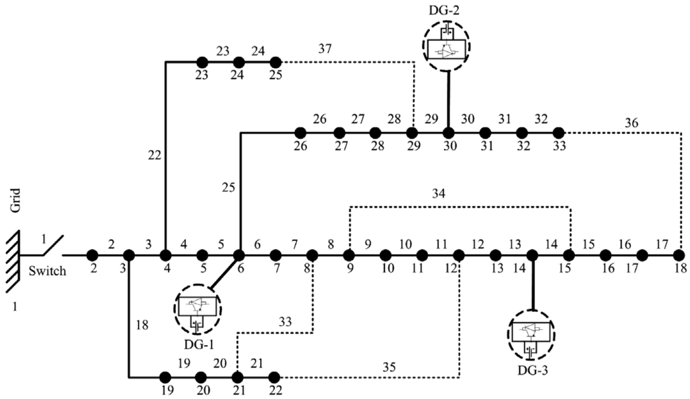

Figure 3. IEEE 33 bus system.

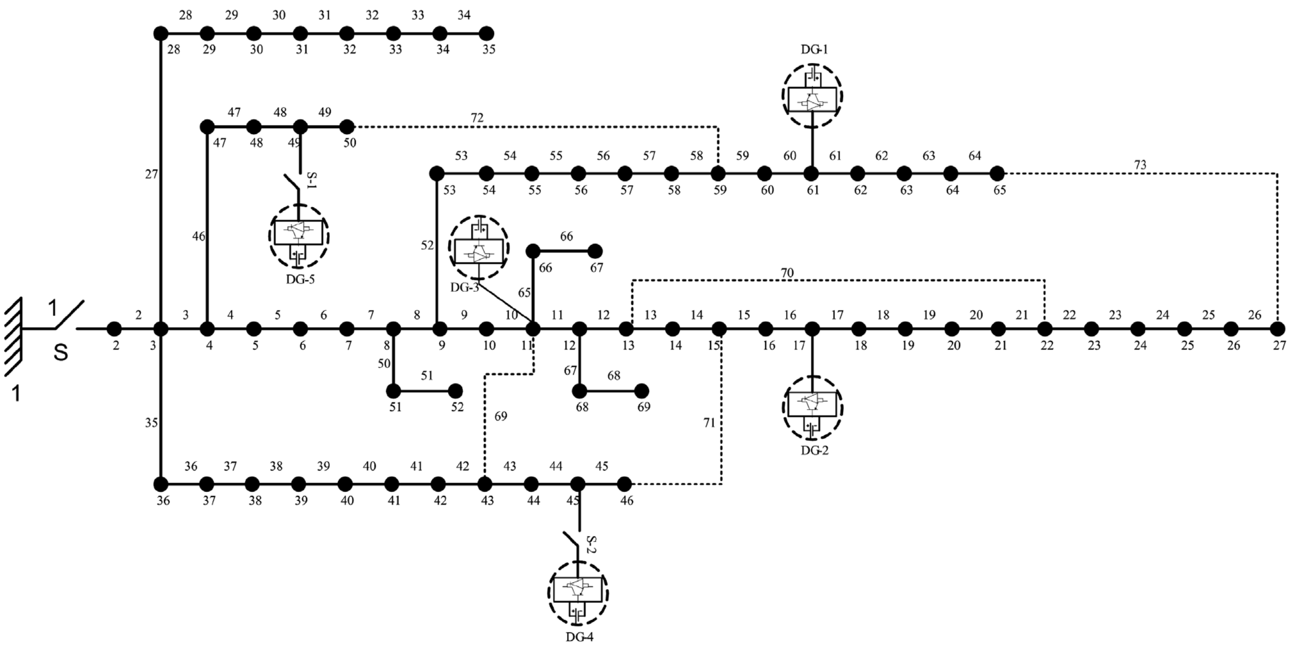

Figure 4. IEEE 69 bus system.

sharing (Q_{exp}) and the percentage error in the reactive power sharing ($Q_{\text{err-}k}$ of kth source) as follows [11]:

$$Q_{\text{exp}} = \frac{Q_1 + Q_2 + \ldots + Q_n}{p} = \frac{Q_{\text{total}}}{p}, \tag{11}$$

$$\% Q_{\text{err}-k} = \frac{Q_k - Q_{\text{exp}}}{Q_{\text{exp}}} \times 100. \tag{12}$$

In the case of unequal source ratings, Q_{exp} can be determined proportionally to the ratings of the sources. Considering a microgrid with three sources having ratings in the ratio of 1:m:n, the expression for Q_{exp} is as follows:

$$Q_{1,\text{exp}} = \frac{Q_{2,\text{exp}}}{m} = \frac{Q_{2,\text{exp}}}{n} = \frac{Q_{\text{total}}}{1+m+n}, \tag{13}$$

where Q_{total} denotes the sum of reactive power of all three DGs. The error in Q_{sh} can be obtained with he help of equation (12) once we get the anticipated reactive power of each DG.

3.1 Low voltage microgrid: test configuration-1

To witness the impact of the proposed DRVVCS, simulation study is performed on test configuration-1, first with common load connected on common ac bus and later on common plus local load-1 connected to DG-1 with switch T_1 closed and common plus local load-2 connected to DG-3 with switch T_2 closed as shown in Figure 1. The control parameters are set to $m_p = 5\text{e}^{-5}$ rad/(W-s), $n_q = 0.5\text{e}^{-3}$ V/VAr and $\beta = 0.03$ for both common load as well as common plus local load.

Simulation result for test configuration-1 with common load is presented in Figure 5 and Table 4. It is to be noted

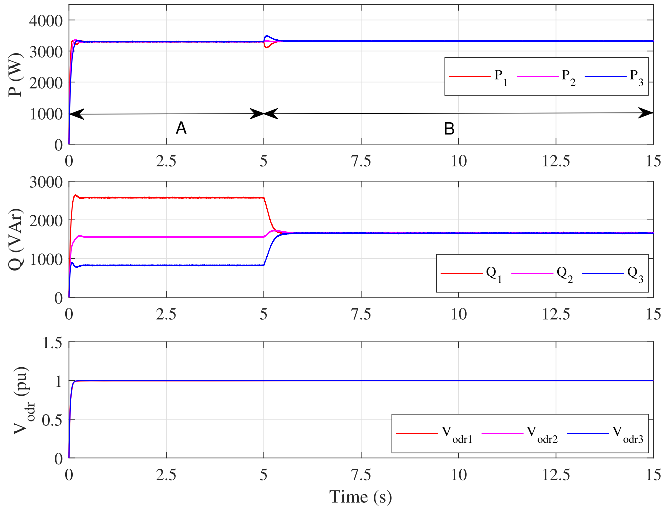

Figure 5. Test Configuration-1 with common load: A = CDCS, B = DRVVCS.

that initially the system is operating in CDCS upto $t = 5$ s, and at $t = 5$ s it dynamically switched to proposed DRVVCS. It can be observed from Figure 5 and Table 4, Q_{err} is very high (54.55%, −2.42%, −51.52%) when sources are operating in CDCS, which reduces to zero after $t = 5$ s when the sources are operating in proposed DRVVCS.

A comprehensive simulation study is also conducted for test configuration-1, involving both common and local loads. The intriguing results, showcased in Figure 6 and Table 4, reveal a remarkable improvement in Q_{sh}. While operating in the conventional CDCS Q_{err} were substantial, reaching as high as (92.42%, −24.24%, −67.68%), when the common load plus local load-1 is connected ($t = 0$ s to $t = 2.5$ s). However, once the sources are transitioned to the proposed DRVVCS, the Q_{err} diminishes to zero ($t = 2.5$ to $t = 7.5$ s). To observe the effect of large reactive power load change on the proposed controller, local load-1 is removed and local load-2 which is purely reactive in nature is connected along with common load ($t = 7.5$ to $t = 10$ s). The Q_{err} in this case is 18.18%, −16.06%, −1.82% while operating in CDCS. Also transients are observed in CDCS which persist for a longer period of time. These transients are mainly due to the large amount of reactive power redistribution among the sources. When the proposed DRVVCS is applied ($t = 10$ to $t = 15$ s), it not only reduces the transients in the response but also shares the reactive power accurately.

To observe the effect of unequal ratings of sources, a simulation study is performed for test system-1 common load case, which is given in Table 4 and Figure 7. In this case, the size of DG-1 is considered to be double the size of DG-2 and DG-3. The control parameters for DG-1 are set to $m_p = 2.5\text{e}^{-5}$ rad/(W-s), $n_q = 2.5\text{e}^{-4}$ V/VAr, while the control parameters for other DGs remain unchanged. It is found from Table 4 and Figure 7 that active power sharing is proportional to the size of DGs, but the Q_{err} is −28.22%, 54.84%, 1.61% when sources are operating in CDCS ($t = 0$ to $t = 5$ s). Proportional active power sharing is achieved in RVVCS also $t = 5$ to $t = 10$ s with reduced Q_{err} (−5.33%, 9.02%, 0.82%). When the sources are operating in proposed DRVVCS ($t = 10$ to $t = 15$ s), the active power sharing as well as reactive power sharing are proportional to the rating of sources, and Q_{err} is zero.

3.2 Low voltage microgrid: Test Configuration-2

To assess the effectiveness of the proposed DRVVCS, a study is carried out on three distinct network topologies, comprising radial, reconfigured, and meshed networks. The simulation studies are then conducted for three distinct cases within the test configuration-2, as illustrated in Figure 2.

- Case-1: Initially, the network is assumed to have a radial nature (S1: closed, S2: open). At $t = 5$ s, the network topology undergoes a dynamic transformation from a radial topology to a reconfigured topology (S1: open, S2: closed). Subsequently, at $t = 10$ s, another dynamic change takes place, transitioning the network topology from the reconfigured topology to a meshed topology (S1: closed, S2: closed). The control parameters are set as follows: $m_p = 1\text{e}^{-4}$ rad/(W-s), $n_q = 5\text{e}^{-4}$ V/VAr, $\beta = 0.03$, $V_n = 380$ V, and $\omega_n = 314.16$ rad/s.
- Case-2: To compare the impact of the proposed DRVVCS, the simulation study is conducted separately for three network configurations: radial network, reconfigured network, and meshed network. At $t = 5$ s, the control strategy dynamically switched from CDCS to the proposed DRVVCS in each network configuration. The controller parameters remain same as with those used in case-1.
- Case-3: The simulation study initially utilizes the RVVCS proposed in [11] . At $t = 2.5$ s, the system dynamically switches to the proposed DRVVCS. At $t = 5$ s, a load of $5 + j\,4$ kVA is disconnected and then reconnected at $t = 7.5$ s to assess the impact of load changes. Subsequently, at $t = 10$ s, the system reverts to the RVVCS when communication fails and dynamically switched to proposed DRVVCS when the communication is restored at $t = 12.5$ s. The controller parameters remain same as with those used in case-1.

3.2.1 Low voltage microgrid: Test Configuration-2 (Case-1)

The proposed (DRVVCS) has been thoroughly validated for robustness using a time-domain simulation platform, with dynamic changes in network topology. The simulations were conducted on three distinct network configurations: a radial topology (T-1), a reconfigured topology (T-2), and a meshed topology (T-3). During the simulations, the active power output (P), reactive power output (Q), and V_{odr} of the sources were closely monitored and shown in Figure 8 and also presented in Table 5. It can be observed that there is a small transient when the network changes from radial topology to reconfigured topology, and from reconfigured topology to meshed topology.

Table 4. CDCS, RVVCS and DRVVCS performance for Low voltage microgrid: Test Configuration-1.

Network configuration	Droop type	$P_{1:3}$ (kW)	$Q_{1:3}$(kVAr)	Q_{exp} (kVAr)	$Q_{\text{err}(1:3)}$ (%)	$v_{\text{odr}(1:3)}$ (pu)
Common load	CDCS	3.30	2.55, 1.61, 0.80	1.65	54.55, −2.42, −51.52	0.996, 0.997, 0.998
	RVVCS	3.16	1.73, 1.6, 1.47	1.6	8.13, 0.00, −8.13	0.980, 0.981, 0.985
	DRVVCS	3.31	1.66, 1.66, 1.66	1.66	0.00, 0.00, 0.00	0.997, 0.999, 1.00
Common + Local Load-1	CDCS	3.95	3.81, 1.50, 0.64	1.98	92.42, −24.24, −67.68	0.994, 0.997, 0.999
	RVVCS	3.80	2.12, 1.84, 1.70	1.89	12.17, −2.65, −10.05	0.971, 0.977, 0.980
	DRVVCS	3.99	2.0, 2.0, 2.0	2.0	0.00, 0.00, 0.00	0.996, 1.003, 1.005
Common + Local Load-2	CDCS	3.30	3.90, 2.77, 3.24	3.30	18.18, −16.06, −1.82	0.994, 0.995, 0.995
	RVVCS	3.12	3.12, 2.97, 3.06	3.05	2.30, −2.62, 0.33	0.954, 0.957, 0.955
	DRVVCS	3.30	3.30, 3.30, 3.30	3.30	0.00, 0.00, 0.00	0.995, 0.998, 0.996
Unequal source rating	CDCS	4.96, 2.48, 2.48	1.78, 1.92, 1.26	2.48, 1.24, 1.24	−28.22, 54.84, 1.61	0.999, 0.996, 0.998
	RVVCS	4.86, 2.43, 2.43	2.31, 1.33, 1.23	2.22, 1.22, 1.22	−5.33, 9.02, 0.82	0.989, 0.986, 0.988
	DRVVCS	4.94, 2.47, 2.47	2.47, 1.24, 1.24	2.47, 1.24, 1.24	0.00, 0.00, 0.00	0.998, 0.995, 0.997

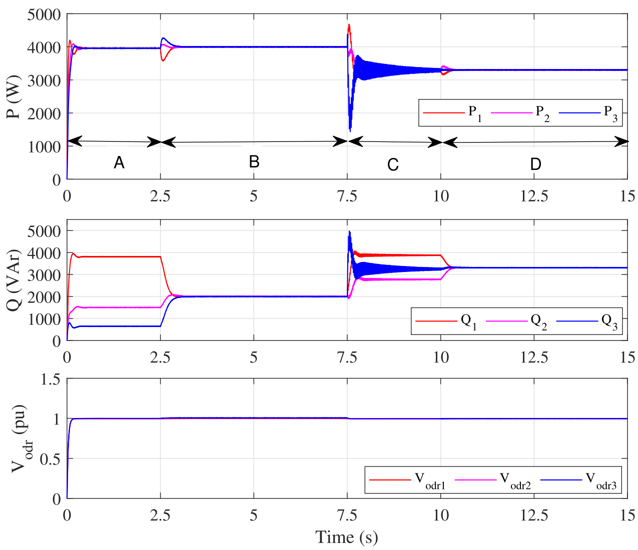

Figure 6. Test Configuration-1 with common plus local load: A = CDCS with local load-1 along with common load, B = DRVVCS with local load-1 along with common load, C = CDCS with local load-2 along with common load, D = DRVVCS with local load-2 along with common load.

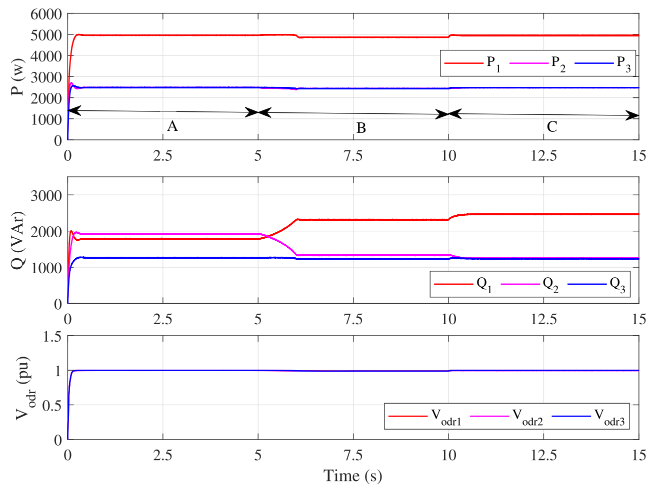

Figure 7. Test Configuration-1 with common load-Unequal source rating: A = CDCS, B = RVVCS, C = DRVVCS.

The proposed DRVVCS work efficiently and Q_{sh} is accurate in each topology.

3.2.2 Low voltage microgrid: Test Configuration-2 (Case-2)

In order to assess the effectiveness of the proposed DRVVCS in comparison to existing CDCS, an extensive simulation is conducted on test configuration-2. This simulation incorporates three distinct network topologies, namely the radial topology, reconfigured topology, and meshed topology. The active power output, reactive power output, and V_{odr} for the radial topology of CDCS and DRVVCS are showcased with utmost clarity in Figure 9 and meticulously detailed in Table 6. It is observed that the error in reactive power sharing (Q_{err}) is high (−28.96%, 36.66%, −7.30%) while operating in CDCS, which is reduced to zero keeping voltage profile close to 1.0 pu, when the control is switched to the proposed DRVVCS. The active power output, reactive power output, and V_{odr} of the reconfigured topology for CDCS and

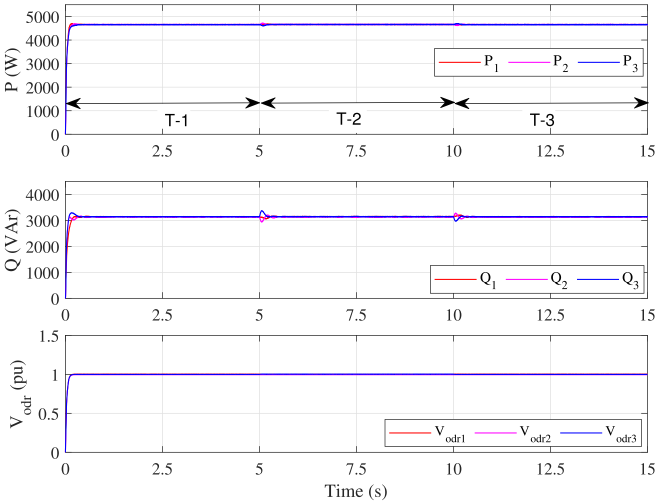

Figure 8. Test Configuration-2 with different network topology operating in DRVVCS: T-1: Radial topology, T-2: Reconfigured topology, T-3: Meshed topology.

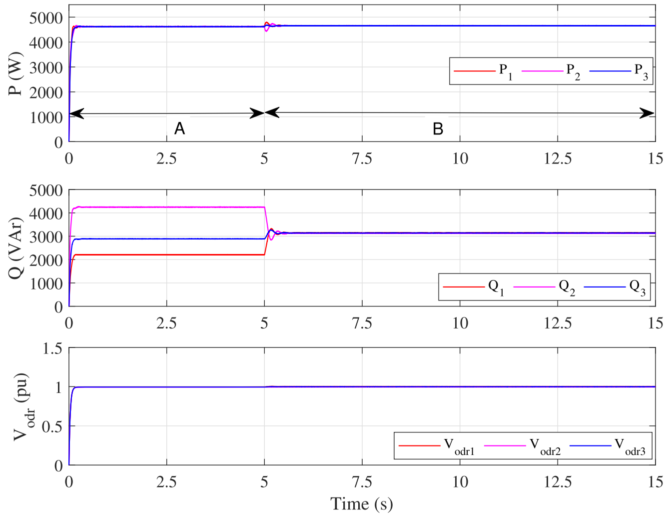

Figure 9. Test Configuration-2 with radial topology: A = CDCS, B = DRVVCS.

Table 5. Test Configuration- 2: Radial topology, reconfigured topology and meshed topology.

Network configuration	$P_{1:3}$ (kW)	$Q_{1:3}$ (kVAr)	Q_{exp} (kVAr)	$Q_{\mathrm{err}(1:3)}$ (%)	$v_{\mathrm{odr}(1:3)}$ (pu)
Radial (T-1)	4.66	3.14, 3.14, 3.14	3.14	0.00, 0.00, 0.00	1.002, 0.995, 0.999
Reconfigured (T-2)	4.66	3.14, 3.14, 3.14	3.14	0.00, 0.00, 0.00	1.002, 0.995, 1.001
Meshed (T-3)	4.66	3.14, 3.14, 3.14	3.14	0.00, 0.00, 0.00	1.002, 0.995, 0.999

Table 6. CDCS, RVVCS and DRVVCS performance of Test Configuration-2 for radial topology, reconfigured topology and meshed topology.

Network configuration	Droop type	$P_{1:3}$ (kW)	$Q_{1:3}$ (kVAr)	Q_{exp} (kVAr)	$Q_{\mathrm{err}(1:3)}$ (%)	$v_{\mathrm{odr}(1:3)}$ (pu)
Radial	CDCS	4.62	2.21, 4.25, 2.88	3.11	−28.96, 36.66, −7.30	0.996, 0.993, 0.995
Topology	RVVCS	4.66	2.91, 3.40, 3.12	3.14	−7.32, 8.28, −0.63	1.00, 0.996, 1.00
	DRVVCS	4.66	3.14, 3.14, 3.14	3.14	0.00, 0.00, 0.00	1.002, 0.995, 0.999
Reconfigured	CDCS	4.62	2.35, 4.55, 2.43	3.11	−24.43, 46.30, −21.87	0.996, 0.993, 0.996
Topology	RVVCS	4.66	2.97, 3.47, 3.0	3.14	−5.41, 10.50, −4.46	1.00, 0.995, 1.00
	DRVVCS	4.66	3.14, 3.14, 3.14	3.14	0.00, 0.00, 0.00	1.002, 0.995, 1.002
Meshed	CDCS	4.62	2.22, 4.27, 2.85	3.11	−28.62, 37.30, −8.36	0.996, 0.993, 0.995
Topology	RVVCS	4.66	2.91, 3.40, 3.11	3.14	−7.32, 8.28, −0.95	1.00, 0.996, 1.00
	DRVVCS	4.66	3.14, 3.14, 3.14	3.14	0.00, 0.00, 0.00	1.002, 0.995, 0.999

DRVVCS is shown in Figure 10 and also presented in Table 6. Q_{err} in this case is −24.43%, 46.30%, −21.87% when the sources are operating in CDCS, but when the proposed DRVVCS is employed the Q_{err} is reduced to zero while maintaining the voltage profile within the limit. Similarly, active power output, reactive power output, and V_{odr} of the meshed topology for CDCS and DRVVCS is shown in Figure 11 and also presented in Table 6. The voltage profile is within the limit and Q_{err} is zero in this case when the sources are operating in the proposed DRVVCS, compared to the Q_{err} of −28.62%, 37.30%, −8.36% in CDCS.

3.2.3 Low voltage microgrid: Test Configuration-2 (Case-3)

In this case test configuration-2 is simulated in meshed topology to evaluate the impact of load variations and communication failures on the on proposed DRVVCS. Furthermore, the compatibility of the suggested controller with other controllers presented in [7, 9–11] is also examined. It can be observed from Figure 12 that initially the system is operating in RVVCS proposed in [11] and dynamically switched to proposed DRVVCS at $t = 2.5$ s. To show the

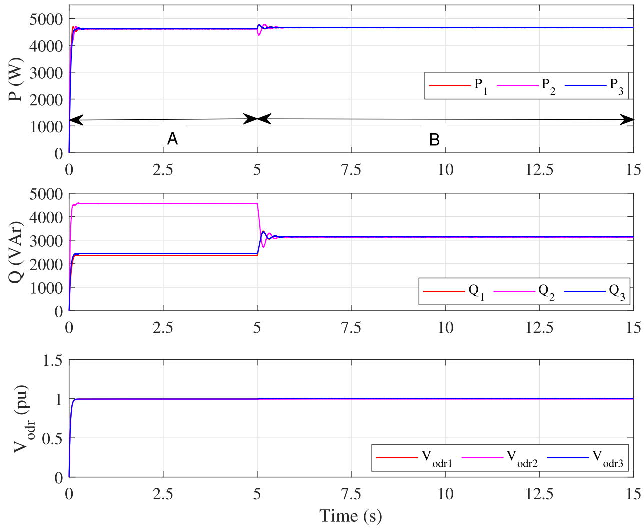

Figure 10. Test Configuration-2 with reconfigured topology: A = CDCS, B = DRVVCS.

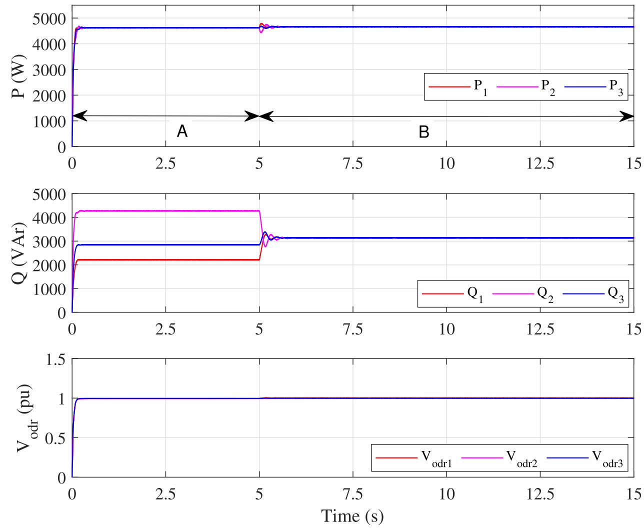

Figure 11. Test Configuration-2 with meshed topology: A = CDCS, B = DRVVCS.

effectiveness and compatibility of the proposed DRVVCS, the RVVCS is chosen in this case, because among all the techniques presented in [7, 9–11], Q_{err} is minimum in RVVCS and the controller is complex. The transition from RVVCS to proposed DRVVCS is seamless and accurate reactive power sharing is achieved by proposed DRVVCS. A similar results are achieved when the proposed DRVVCS operates alongside the controllers from [7, 9 and 10], which shows its compatibility with other controllers. Upon removing a load of $5 + j\,4$ kVA at $t = 5$ s and subsequently reconnecting it at $t = 7.5$ s, a transient response is observed due to the substantial alteration in reactive power output. However, the proposed DRVVCS accurately shares reactive power during these load changes. In the event of a communication failure at $t = 12.5$ s, the system dynamically shifts to the RVVCS mode, functioning in a decentralized manner until communication is re-established at $t = 12.5$ s.

3.3 Standard IEEE system

This study is also performed for standard IEEE 33-bus system and standard IEEE 69-bus system. The control parameters for IEEE 33-bus system are $m_p = 2\text{e}^{-7}$ rad/(W-s), $n_q = 1\text{e}^{-4}$ V/VAr, $\beta = 0.015$, $V_n = 12.66$ kV, and $\omega_n = 314.16$ rad/s and for IEEE 69-bus system are $m_p = 0.25\text{e}^{-6}$ rad/(W-s), $n_q = 1\text{e}^{-4}$ V/VAr, $\beta = 0.015$, $V_n = 12.66$ kV, and $\omega_n = 314.16$ rad/s.

3.3.1 Standard IEEE 33-bus system

The proposed DRVVCS is tested on standard IEEE 33-bus system to observed the performance on practical system. The result obtained is shown in Figure 13 and Table 7. Three DGs of equal rating are connected at bus no. 14, 24 and 31. Initially all DGs are operating in CDCS from $t = 0$ s to $t = 2$ s, the Q_{err} is 88.29%, 3.63%, −91.92%. From $t = 2$ s to $t = 3$ s, there is transition from CDCS to RVVCS and at $t = 3$ s sources are operating in RVVCS, which reduces Q_{err} to 11.79%, 6.00%, −17.80% but reactive power sharing is still not accurate. When DGs are dynamically switched to the proposed DRVVCS at $t = 4$ s the (Q_{err}) reduces to almost zero giving accurate reactive power sharing among the sources while keeping the voltage profile within the permissible limit. It was observed that large transients occurs in case of sudden change from CDCS to DRVVCS because of large redistribution of reactive power. In this study, a gradual transition from CDCS to RVVCS is employed to minimize transients ($t = 2$ s to $t = 3$ s). However, Figure 14 portray that the operation with proposed DRVVCS is smooth. This study is also conducted for randomly chosen different location where the Distributed Generators (DGs) are connected to buses 6, 30, and 14, demonstrating the independence of the proposed method from DG placement. DGs locations are further changed to buses 3, 6, and 29. A similar result is achieved in each scenario.

3.3.2 Standard IEEE 69-bus system

The simulation study also includes the analysis of the standard IEEE 69-bus system. In this scenario, two cases has been considered. In first case, three DGs with equal ratings are connected to buses 61, 17, and 11, and in second case, five DGs with equal ratings are connected to buses 61, 17, 11, 45, and 49. The corresponding results are presented in Tables 8 and 9 respectively . Figure 15 illustrates the outcomes when five DGs are connected.

It is observed that in the case of three sources operating in CDCS, the Q_{err} is notably high "136.62%, −157.47%, 20.86%", and reduced to "20.48%, −20.75%, 0.267%" when dynamically swiched to RVVCS. The (Q_{err}) significantly reduces to almost zero when the proposed technique is

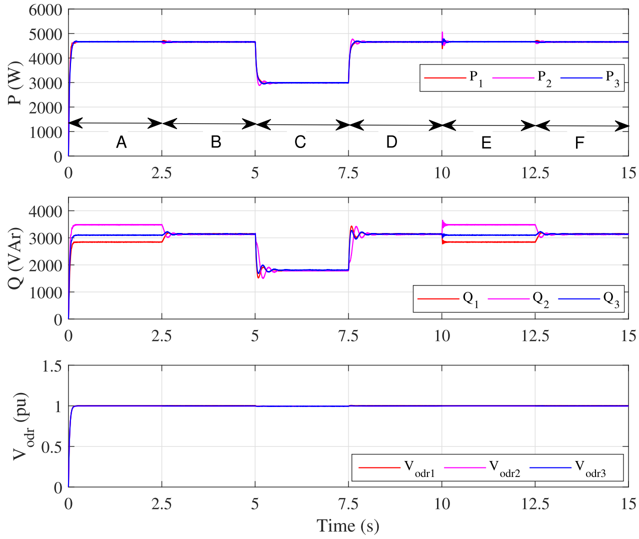

Figure 12. Test Configuration-2 with meshed topology during load change and communication failure: A, E = RVVCS & B, C, D, F = DRVVCS, C = Load Removed, D = Load reconnected, E = Communication failure, F = Communication restored.

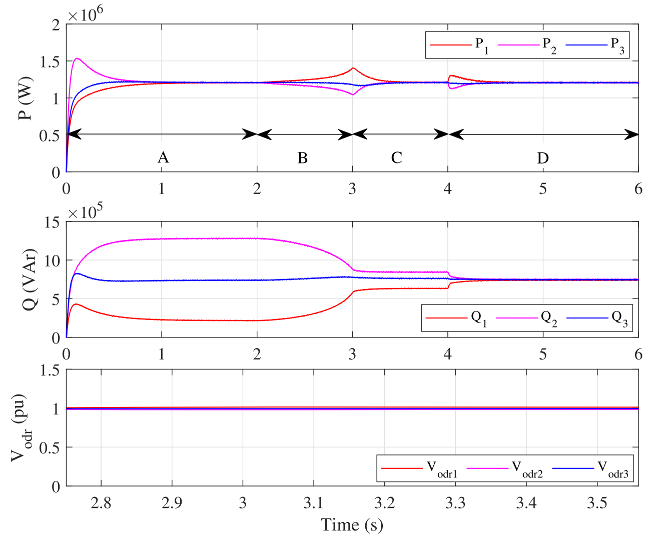

Figure 13. Standard IEEE 33-bus system: A = CDCS, B = Transition from CDCS to RVVCS, C = RVVCS, D = DRVVCS.

Table 7. CDCS and DRVVCS performance for standard IEEE 33-bus system.

DG location	Droop type	$P_{1:3}$ (MW)	$Q_{1:3}$ (MVAr)	Q_{exp} (MVAr)	$Q_{err(1:3)}$ (%)	$v_{odr(1:3)}$ (pu)
DG-1,2,3 (6,30,14)	CDCS	1.19	1.399, 0.77, 0.06	0.743	88.29, 3.63, −91.92	0.9776, 0.9847, 0.9918
	RVVCS	1.19	0.831, 0.788, 0.611	0.743	11.79, 6.00, −17.80	0.997, 0.983, 1.008
	DRVVCS	1.14	0.716, 0.71, 0.698	0.708	1.12, 0.28, −1.41	0.9524, 0.9584, 0.9861
DG-1,2,3 (14,24,31)	CDCS	1.20	0.217, 1.28, 0.742	0.746	−70.92, 71.51, −0.58	0.9917, 0.9806, 0.9864
	RVVCS	1.20	0.633, 0.845, 0.76	0.746	−15.15, 13.27, 1.88	1.006, 0.976, 0.986
	DRVVCS	1.20	0.738, 0.751, 0.744	0.744	−0.85, 0.89, −0.04	1.007, 0.9717, 0.9841
DG-1,2,3 (3,6,29)	DRVVCS	1.22	0.780, 0.722, 0.740	0.750	4.0, −3.73, −1.33	0.989, 0.993, 0.997

applied. In case of five DGs in operation, during CDCS (t = 0 s to t = 2 s), the Q_{err} is very high "281.94%, −144.81%, −41.95%, −96.71%, 1.53%". There is a transition period from t = 2 s to t = 3 s, where control strategy is shifting gradually from CDCS to RVVCS. At t = 3 s RVVCS is fully functional and Q_{err} decreases to "40.46%, −20.40%, −4.37%, −13.45%, −2.24%", but proportional reactive power is not achieved. However, when the DGs dynamically switch to the proposed DRVVCS (t = 4 s to t = 6 s), the Q_{err} is reduced to almost zero, and proportional reactive power sharing among the sources is accomplished. Large transients were observed in this case while sudden switching from CDCS to RVVCS, which is reduced by gradual shifting from CDCS to RVVCS (t = 2 s to t = 3 s). When the system is operating with the proposed DRVVCS, it gives smooth response as illustrated in Figure 16. To observe the effect of change in locations of DGs, a simulation study is also conducted when the DGs are connected to buses 3, 26, and 58, and buses 9, 23, and 43. The performance of the proposed DRVVCS is satisfactory, and the Q_{err} is nearly zero for each location.

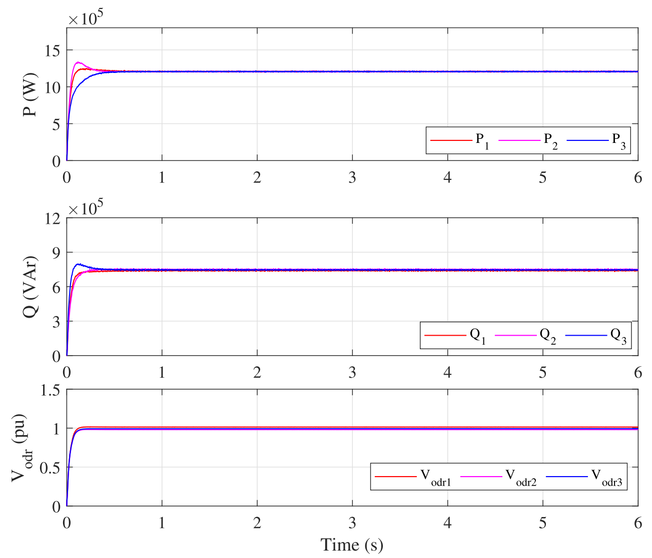

Figure 14. Standard IEEE 33-bus system: DRVVCS.

Table 8. CDCS and DRVVCS performance for standard IEEE 69-bus system: Three DGs.

DG location	Droop type	$P_{1:3}$ (MW)	$Q_{1:3}$ (MVAr)	Q_{exp} (MVAr)	$Q_{\mathrm{err}(1:3)}$ (%)	$v_{\mathrm{odr}(1:3)}$ (pu)
DG-1,2,3 (61,17,11)	CDCS	1.25	2.042, −0.496, 1.043	0.863	136.62, −157.47, 20.86	0.971, 0.998, 0.981
	RVVCS	1.2	1.009, 0.664, 0.839	0.837	20.48, −20.75, 0.267	0.955, 1.004, 0.978
	DRVVCS	1.22	0.859, 0.848, 0.85	0.852	0.78, −0.51, −0.27	0.959, 1.009, 0.982
DG-1,2,3 (3,26,58)	DRVVCS	1.25	0.867, 0.863, 0.876	0.868	−0.12, −0.57, 0.92	0.992, 1.04, 0.981
DG-1,2,3 (9,23,43)	DRVVCS	1.25	0.870, 0.857, 0.855	0.860	1.62, −0.34, −0.58	0.992, 1.03, 1.009

Table 9. CDCS and DRVVCS performance for standard IEEE 69-bus system: Five DGs.

DG location	Droop type	$P_{1:5}$ (MW)	$Q_{1:5}$ (MVAr)	Q_{exp} (MVAr)
DG-1,2,3,4,5 (61,17,11,45,49)	CDCS	0.755	2.02, −0.237, 0.307, 0.017, 0.537	0.529
	RVVCS	0.735	0.727, 0.412, 0.495, 0.448, 0.506	0.518
	DRVVCS	0.755	0.54, 0.505, 0.521, 0.508, 0.513	0.517
DG location	Droop type	$Q_{err(1:5)}$ (%)	$v_{odr(1:5)}$ (pu)	
DG-1,2,3,4,5 (61,17,11,45,49)	CDCS	281.94, −144.81, −41.95, −96.71, 1.53	0.981, 1.002, 0.997, 0.999, 0.995	
	RVVCS	40.46, −20.40, −4.37, −13.45,−2.24	0.963, 1.006, 0.995, 1.002, 0.992	
	DRVVCS	4.37, −2.39, 0.695, −1.82, −0.85	0.961, 1.007, 0.995, 1.003, 0.992	

4 Multiplication Factor (M_{fc}) and Tuning of Control Parameter (β)

The M_{fc} is common for each DG and adapts based on load changes. The nature of M_{fc} is such that it maintains the factor γM_{fc} close to 1.0 under varying loads, thus ensuring the voltage profile remains within the desired limit. The generation of M_{fc} can originate from any DG and is then transmitted to all other DGs through a low bandwidth, one way communication channel. This approach greatly improves system flexibility and scalability. Importantly, the generation of M_{fc} relies solely on information from the specific DG that produces it; neighbouring source information is not required for this process which further reduces the communication dependency. To show the effect of M_{fc} from different DGs on the reactive power sharing performance of DRVVCS, M_{fc} is generated by DG-1 from $t = 0$ s to $t = 5$ s. From $t = 5$ s to $t = 10$ s, M_{fc} is generated by DG-2, and from $t = 10$ s to $t = 15$ s, M_{fc} is generated by DG-3. Figure 17 and Table 10 illustrates that in each scenario, accurate sharing of reactive power is achieved while upholding the voltage profile at approximately 1.0 pu. Control parameter β is selected by making a trade off between speed of response and oscillations. By reducing the value of β the system response becomes fast, but this can introduce escalating oscillations in the response. These oscillations intensify with diminishing β values and could potentially drive the system toward instability. Furthermore, with increasing loads, the upper threshold for β, allowing stable operation, also rises; however, setting β too high results in sluggish responses. Therefore, the selection of β must strike a compromise where the system response is adequately fast while maintaining overall stability. The variation in

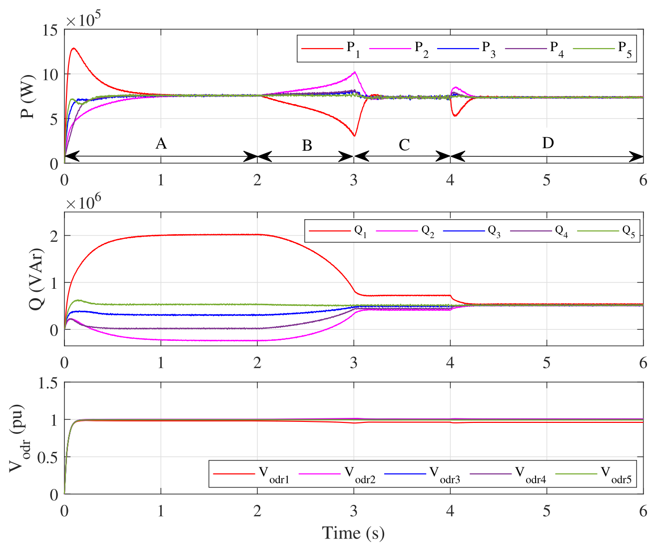

Figure 15. Standard IEEE 69-bus system: A = CDCS, B = Transition from CDCS to RVVCS, C = RVVCS, D = DRVVCS.

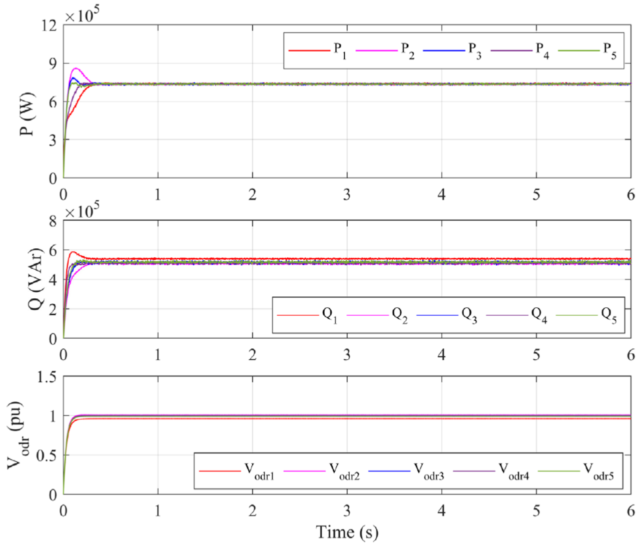

Figure 16. Standard IEEE 69-bus system: DRVVCS.

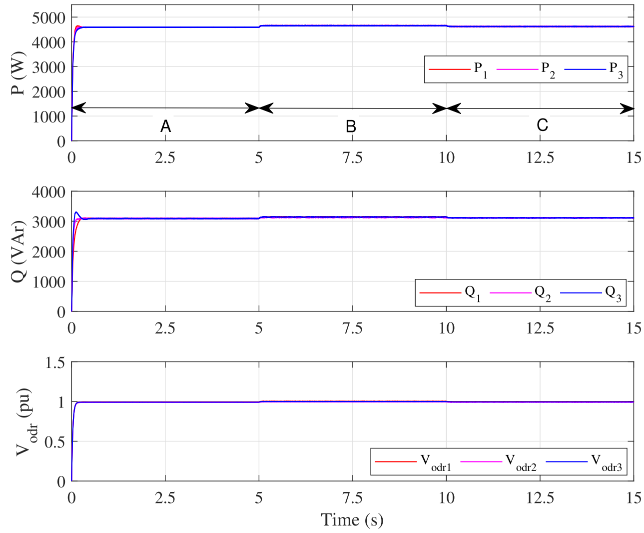

Figure 17. Test Configuration-2 with meshed topology during various multiplication factor: A = M_{fc} by DG-1, B = M_{fc} by DG-2, C = M_{fc} by DG-3.

Table 10. DRVVCS performance of test Configuration-2 for meshed topology under various M_{fc}.

M_{fc} generating DG	$P_{1:3}$ (kW)	$Q_{1:3}$ (kVAr)	Q_{exp} (kVAr)	$Q_{err(1:3)}$ (%)	$v_{odr(1:3)}$ (pu)
DG-1	4.58	3.10, 3.10, 3.10	3.10	0.00, 0.00, 0.00	0.995, 0.988, 0.992
DG-2	4.66	3.14, 3.14, 3.14	3.14	0.00, 0.00, 0.00	1.002, 0.995, 0.999
DG-3	4.62	3.11, 3.11, 3.11	3.11	0.00, 0.00, 0.00	0.998, 0.991, 0.995

Table 11. Variation in overshoot and settling time with β.

β	Settling time ($Q_{1:3}$) (s)	Overshoot ($Q_{1:3}$) (%)
0.01	1.7158, 1.9959, 1.6854	6.3973, 137.5658, 6.9922
0.03	0.4038, 0.5340, 0.3945	3.1644, 12.5940, 11.9193
0.05	0.3421, 0.4935, 0.3228	3.5549, 9.7772, 17.1256
0.07	0.4048, 0.4044, 0.2374	5.2045, 6.9302, 20.1601
0.09	0.4688, 0.4511, 0.2824	5.8702, 4.9918, 21.8763
0.1	0.4994, 0.4606, 0.3138	6.3520, 3.9276, 22.5939
0.2	0.7673, 0.4574, 0.7316	7.5689, 0.5056, 25.8237
0.3	0.9798, 0.7364, 1.0349	7.6988, 0.3896, 26.4954
0.4	0.9006, 0.9392, 1.2226	8.0028, 0.2841, 26.5193
1.0	0.5873, 1.4106, 1.4916	8.7539, 0.1520, 24.7386

overshoot and settling time with β for test system-2 with meshed configuration is presented in Table 11.

5 Conclusion

In this research paper, we addressed the challenges of achieving accurate proportional reactive power sharing among distributed energy resources within islanded microgrids. A novel Distributed Robust Volt-VAr Control Strategy(DRVVCS) that effectively bridges the gap between existing decentralized and centralized control methods is proposed. Through extensive simulations across various network topologies, load variations, and communication scenarios, we demonstrated the robustness and adaptability of the proposed DRVVCS.

Results obtained from MATLAB Simulink showcased that the DRVVCS outperforms conventional droop control in terms of proportional reactive power sharing accuracy, while maintaining voltage profile within desired limit. The proposed scheme's compatibility with other controllers and its ability to respond to load changes further underscore its practical applicability. This study conducted both the standard IEEE 33-bus system and the IEEE 69-bus system establishes that the proposed control method is equally effective when applied to practical systems. In case of DG maintenance, system expansion, or DG failure, the proposed DRVVCS operates effectively, as M_{fc} can be generated by any DG, enhancing its flexibility and scalability. The control parameter β was carefully tuned to ensure a balance between speed of response and system stability. The proposed DRVVCS addresses the limitations of existing methods, shares reactive power accurately among DGs, provides adaptability, and minimizes communication dependency, thereby contributing to the efficient and resilient operation of islanded microgrid systems. In case of communication failure, the proposed DRVVCS changes its control to RVVCS in which some amount of error in reactive power exist, which is a limitation of the proposed strategy. The proposed DRVVCS can be designed to operate in a decentralized manner in the future to overcome the existing limitation.

Acknowledgments

The authors sincerely acknowledge NIT Patna for allowing the research to be undertaken.

Funding

This research did not receive any specific grant from funding agencies in the public, commercial, or not-for-profit sectors.

Conflicts of interest

The authors declare that they have no competing financial interests or personal relationships that could have appeared to influence the work reported in this paper.

Data availability statement

No data was used for the research described in this article.

Author contribution statement

The manuscript is written through contributions of all authors.

Pradeep Kumar Singh: Conceptualization, Methodology, Software, Data curation, Writing- Original draft preparation, Validation.

Dharmendra Kumar Dheer: Visualization, Investigation, Supervision, Writing- Reviewing and Editing.

References

1 Manzoor A., Akram W., Judge M.A., Khan N., Khattak H.A. (2024) Efficient economic energy scheduling in smart cities using distributed energy resources, *Sci. Technol. Energy Trans.* **79**, 29.

2 Majid S.H., Alkhayer A.G., Askar S., Rajiv A., Singh S., Kaur S., Singh A., Hussein L., Romaina Y.S., Perz R. (2024) Modelling cost-effective of electric vehicles and demand response in smart electrical microgrids, *Sci. Technol. Energy Trans.* **79**, 63.

3 Ahmed K., Seyedmahmoudian M., Mekhilef S., Mubarak N., Stojcevski A. (2020) A review on primary and secondary controls of inverter-interfaced microgrid, *J. Mod. Power Syst. Clean Energy* **9**, 5, 969–985.

4 Olivares D.E., Mehrizi-Sani A., Etemadi A.H., Cañizares C. A., Iravani R., Kazerani M., Hajimiragha A.H., Gomis-Bellmunt O., Saeedifard M., Palma-Behnke R., et al. (2014) Trends in microgrid control, *IEEE Trans. Smart Grid* **5**, 4, 1905–1919.

5 Guerrero J.M., Chandorkar M., Lee T.L., Loh P.C. (2012) Advanced control architectures for intelligent microgrids – Part I: Decentralized and hierarchical control, *IEEE Trans. Ind. Electron.* **60**, 4, 1254–1262.

6 Guerrero J.M., Loh P.C., Lee T.L., Chandorkar M. (2012) Advanced control architectures for intelligent microgrids – part II: Power quality, energy storage, and ac/dc microgrids, *IEEE Trans. Ind. Electron.* **60**, 4, 1263–1270.

7 Chandorkar M.C., Divan D.M., Adapa R. (1993) Control of parallel connected inverters in standalone ac supply systems, *IEEE Trans. Ind. Appl.* **29**, 1, 136–143.

8 Pogaku N., Prodanovic M., Green T.C. (2007) Modeling, analysis and testing of autonomous operation of an inverter-based microgrid, *IEEE Trans. Power Electron.* **22**, 2, 613–625.

9 Dheer D.K., Gupta Y., Doolla S. (2019) A self-adjusting droop control strategy to improve reactive power sharing in islanded microgrid, *IEEE Trans. Sustain. Energy* **11**, 3, 1624–1635.

10 Dheer D.K., Gupta Y., Doolla S. (2021) Decentralised inverter control for improved reactive power sharing and voltage profile in a microgrid*, IET Gener. Transm. Distrib.* **15**, 7, 1227–1241.

11 Singh P.K., Dheer D.K. (2023) Robust Volt-VAr control strategy for improvement in reactive power sharing in a droop based islanded microgrid, *Arab. J. Sci. Eng.* **48**, 1, 15495–15508.

12 Ling Y., Li Y., Yang Z., Xiang J. (2020) A dispatchable droop control method for distributed generators in islanded ac microgrids, *IEEE Trans. Ind. Electron.* **68**, 9, 8356–8366.

13 Gupta Y., Chatterjee K., Doolla S. (2020) A simple control scheme for improving reactive power sharing in islanded microgrid, *IEEE Trans. Power Systems* **35**, 4, 3158–3169.

14 Aquib M., Parth N., Doolla S., Chandorkar M.C. (2023) An adaptive droop scheme for improving transient and steady-state power sharing among distributed generators in islanded microgrids, *IEEE Trans. Ind. Appl.* **59**, 4, 5136–5148.

15 Liu B., Liu Z., Liu J., An R., Zheng H., Shi Y. (2019) An adaptive virtual impedance control scheme based on small-ac-signal injection for unbalanced and harmonic power sharing in islanded microgrids, *IEEE Trans. Power Electron.* **34**, 12, 12333–12355.

16 Minetti M., Rosini A., Denegri G.B., Bonfiglio A., Procopio R. (2021) An advanced droop control strategy for reactive power assessment in islanded microgrids. *IEEE Trans. Power Systems* **37**, 4, 3014–3025.

17 Pham X.H.T. (2021) An improved controller for reactive power sharing in islanded microgrid, *Elec. Eng.* **103**, 3, 1679–1689.

18 Nookala S., Shiva C.K., Basetti V. (2024) Enhancing decentralized frequency regulation approach in mixed source of generation diversified with wind and PV integration deploying artificial gorilla troops algorithm, *Sci. Technol. Energy Trans.* **79**, 52.

19 Gao Z. (2024) Study on frequency stability control strategies for microgrid based on hybrid renewable energy, *Sci. Technol. Energy Trans.* **79**, 54.

20 Mousavi S.Y.M., Jalilian A., Savaghebi M., Guerrero J.M. (2018) Autonomous control of current-and voltage-controlled dg interface inverters for reactive power sharing and harmonics compensation in islanded microgrids, *IEEE Trans. Power Electron.* **33**, 11, 9375–9386.

21 He J., Li Y.W. (2011) Analysis, design, and implementation of virtual impedance for power electronics interfaced distributed generation, *IEEE Trans. Ind. Appl.* **47**, 6, 2525–2538.

22 He J., Li Y.W. (2010) Analysis and design of interfacing inverter output virtual impedance in a low voltage microgrid, in: *2010 IEEE Energy Conversion Congress and Exposition*, IEEE, pp. 2857–2864.

23 Cao W., Han M., Zhang X., Xie W., Agundis-Tinajero G.D., Guerrero J.M. (2020) A novel power sharing scheme of controlling parallel-operated inverters in islanded microgrids', *IEEE J. Emerg. Sel. Top. Power Electron.* **9**, 5, 5732–5746.

24 Vijay A., Parth N., Doolla S., Chandorkar M.C. (2021) An adaptive virtual impedance control for improving power sharing among inverters in islanded ac microgrids, *IEEE Trans. Smart Grid* **12**, 4, 2991–3003.

25 Deng F., Li X., Zhang X., Mattavelli P. (2021) An iterative virtual impedance regulation strategy in islanded microgrids for enhanced balanced, unbalanced and harmonic current sharing, *IEEE Trans. Sustain. Energy* **13**, 1, 514–526.

26 Khan I., Vijay A., Doolla S. (2023) Evaluating power sharing performance of distributed generators in microgrids with hybrid sources and mixed tie-lines, *IEEE Trans. Ind. Appl.* **59**, 5, 5363–5375.

27 Pournazarian B., Seyedalipour S.S., Lehtonen M., Taheri S., Pouresmaeil E. (2020) Virtual impedances optimization to enhance microgrid small-signal stability and reactive power sharing, *IEEE Access* **8**, 139691–139705.

28 Li Y.W., Kao C.N. (2009) An accurate power control strategy for power-electronics-interfaced distributed generation units operating in a low-voltage multibus microgrid, *IEEE Trans. Power Electron.* **24**, 12, 2977–2988.

29 Mohammed N., Lashab A., Ciobotaru M., Guerrero J.M. (2022) Accurate reactive power sharing strategy for droop-based islanded ac microgrids, *IEEE Trans. Ind. Electron.* **70**, 3, 2696–2707.

30 Guerrero J.M., De Vicuna L.G., Matas J., Castilla M., Miret J. (2005) Output impedance design of parallel-connected ups inverters with wireless load-sharing control, *IEEE Trans. Ind. Electron.* **52**, 4, 1126–1135.

31 He J., Li Y.W. (2012) An enhanced microgrid load demand sharing strategy, *IEEE Trans. Power Electron.* **27**, 9, 3984–3995.

32 Pham M.D., Lee H.H. (2020) Effective coordinated virtual impedance control for accurate power sharing in islanded microgrid, *IEEE Trans. Ind. Electron.* **68**, 3, 2279–2288.

33 Hoang T.V., Lee H.H. (2020) Virtual impedance control scheme to compensate for voltage harmonics with accurate harmonic power sharing in islanded microgrids, *IEEE J. Emerg. Sel. Top. Power Electron.* **9**, 2, 1682–1695.

34 Wong Y.C.C., Lim C.S., Cruden A., Rotaru M.D., Ray P.K. (2020) A consensus-based adaptive virtual output impedance control scheme for reactive power sharing in radial microgrids, *IEEE Trans. Ind. Appl.* **57**, 1, 784–794.

35 Zhou J., Tsai M.J., Cheng P.T. (2019) Consensus-based cooperative droop control for accurate reactive power sharing in islanded ac microgrid, *IEEE J. Emerg. Sel. Top. Power Electron.* **8**, 2, 1108–1116.

36 Duarte J., Velasco M., Mart P., Camacho A., Miret J., Alfaro C. (2022) Decoupled simultaneous complex power sharing and voltage regulation in islanded ac microgrids, *IEEE Trans. Ind. Electron.* **70**, 4, 3888–3898.

37 Babayomi O., Li Y., Zhang Z. (2022) Distributed consensus-based reactive power sharing in microgrids: A predictive virtual capacitance control technique, *Int. J. Electr. Power Energy Syst.* **141**, 108139.

38 Qian H., Xu Q., Du P., Xia Y., Zhao J. (2020) Distributed control scheme for accurate power sharing and fixed frequency operation in islanded microgrids, *IEEE Trans. Ind. Electron.* **68**, 12, 12229–12238.

39 Lu J., Zhao M., Golestan S., Dragicevic T., Pan X., Guerrero J.M. (2021) Distributed event-triggered control for reactive, unbalanced, and harmonic power sharing in islanded ac microgrids, *IEEE Trans. Ind. Electron.* **69**, 2, 1548–1560.

40 Jasim A.M., Jasim B.H., Aymen F., Kotb H., Althobaiti A., et al. (2023) Consensus-based intelligent distributed secondary control for multiagent islanded microgrid, *Int. Trans. Electr. Energy Syst.* **2023**, 6812351.

41 Han R., Meng L., Ferrari-Trecate G., Coelho E.A.A., Vasquez J.C., Guerrero J.M. (2017) Containment and consensus-based distributed coordination control to achieve bounded voltage and precise reactive power sharing in islanded ac microgrids, *IEEE Trans. Ind. Appl.* **53**, 6, 5187–5199.

42 Hou S., Chen J., Chen G. (2023) Distributed control strategy for voltage and frequency restoration and accurate reactive power-sharing for islanded microgrid, *Energy Rep.* **9**, 742–751.

43 Wan X., Wu J. (2022) Distributed hierarchical control for islanded microgrids based on adjustable power consensus, *Electronics* **11**, 3, 324.

44 Kim S., Hyon S., Kim C. (2018) Distributed virtual negative-sequence impedance control for accurate imbalance power sharing in islanded microgrids*, Sustain. Energy Grids Netw.* **16**, 28–36.

45 Xu Y., Guo Q., Sun H., Fei Z. (2018) Distributed discrete robust secondary cooperative control for islanded microgrids, *IEEE Trans. Smart Grid* **10**, 4, 3620–3629.

46 Mottaghizadeh M., Aminifar F., Amraee T., Sanaye-Pasand M. (2021) Distributed robust secondary control of islanded microgrids: Voltage, frequency, and power sharing, *IEEE Trans. Power Delivery* **36**, 4, 2501–2509.

47 Chen Y., Lao K.W., Qi D., Hui H., Yang S., Yan Y., Zheng Y. (2023) Distributed self-triggered control for frequency restoration and active power sharing in islanded microgrids, *IEEE Trans. Ind. Informat.* **19**, 10, 10635–10646.

48 Venkatesh B., Ranjan R., Gooi H. (2004) Optimal reconfiguration of radial distribution systems to maximize loadability, *IEEE Trans. Power Systems* **19**, 1, 260–266.

49 Savier J., Das D. (2007) Impact of network reconfiguration on loss allocation of radial distribution systems, *IEEE Trans. Power Delivery* **22**, 4, 2473–2480.